ELSEVIER

Journal of Alloys and Compounds 279 (1998) 252–258

Journal of ALLOYS AND COMPOUNDS

Effect of heat treatment on the corrosion behaviour of amorphous Mg-18 at% Ni alloy

M.S. Ong[a], Y. Li[a,*], D.J. Blackwood[a], S.C. Ng[b], C.H. Kam[a]

[a]*Department of Materials Science, National University of Singapore, Singapore 119260, Singapore*
[b]*Department of Physics, National University of Singapore, Singapore 119260, Singapore*

Received 28 April 1998

Abstract

The effect of heat treatment on the corrosion resistance of rapidly solidified amorphous $Mg_{82}Ni_{18}$ ribbons has been studied by hydrogen evolution testing in 3% NaCl solution and potentiodynamic scanning in 0.01 M NaCl solution. The results show that the dissolution rate for the partially crystallised sample obtained after 4 min heat treatment at 160°C, was lower in comparison to the fully crystalline or fully amorphous samples. Comparison of the polarisation responses of the samples showed that, for the partially crystallised samples, passivation current density was lower than that of the fully amorphous sample, although passivation behaviour was weaker. With prolonged heat treatment duration, fully crystallised samples exhibited a marked deterioration of corrosion resistance. The corrosion results were discussed and correlated with the progress of crystallisation processes by means of XRD, DSC, TEM and SEM.

Keywords: Heat treatment; Mg–Ni alloy; Hydrogen Evolution Testing; Electrochemical; Amorphous

1. Introduction

It is well known that very high purity metals have higher corrosion resistances than otherwise, since their uniformity makes it difficult for specific anodic and cathodic sites to develop on their surfaces. Crystal lattices are thermodynamically more stable than amorphous structures, and hence crystallisation might be expected to reduce the corrosion rate, particularly in the case of single crystals. Any such beneficial effects are usually offset, however, by the development of inhomogeneity in the metal surface that allow the establishment of cathodic and anodic sites. For example, the stable crystalline grains may act as cathodes causing accelerated corrosion of the less stable, and thus anodic, grain boundaries, or alternatively if different crystal phases are present the more stable phases will become cathodes and the less stable ones anodes. These effects are even greater in alloys where crystals of different chemical composition will be formed. These effects are similar to galvanic corrosion, except both anodes and cathodes are formed within the same metal, and are often referred to as microgalvanic coupling.

The poor corrosion resistance of crystalline Mg alloys is partly the result of alloy additions and the presence of impurities [1]. However, with the use of rapid solidification processing to form of a chemically homogeneous structure, an enhanced corrosion resistance of Mg-based alloys has been reported [2–14]. Moreover, recently corrosion resistant amorphous Mg-based metallic glasses containing rare-earths, Ni and Cu additions have also been reported [10–14].

However, the chemical heterogeneity caused by crystallisation, precipitation and segregation during thermal exposure can cause a marked deterioration in the corrosion resistance [12]. Thus, the successful use of amorphous Mg-based alloys depends on developing an understanding of the response of their corrosion behaviour towards heat treatment. Hence, the present work aims to study the corrosion behaviour of rapidly solidified Mg–Ni binary alloy containing 18at% Ni addition before and after heat treatment using hydrogen evolution testing and an anodic polarisation test. The results are correlated with the crystallisation result from heat treatment and studied by

*Corresponding author. Tel.: +65 777 2603; fax: +65 777 6126.

0925-8388/98/$ – see front matter
PII: S0925-8388(98)00679-3

means of X-ray diffraction (XRD), differential scanning calorimetry (DSC) and transmission electron microscopy (TEM).

2. Experimental

$Mg_{82}Ni_{18}$ ribbons were prepared by chill block melt-spinning carried out under argon, the chamber having been evacuated to a pressure less than 2×10^{-2} mbar before back-filling with argon. The melt expulsion nozzle bore was 0.7 mm and the wheel speed was 30 m s^{-1}. Heat treatments of the resulting ribbons were carried out in quartz tubes evacuated before back-filling with argon. The samples were heat treated at 160°C for 4, 6, 10, 30 and 60 min respectively, with the heat treatments terminated by water quenching. The amorphous state and crystalline phases obtained after heat treatment were confirmed by XRD using Cu K_α radiation, DSC and TEM.

Corrosion resistance of the alloys was evaluated by a hydrogen evolution testing method [2,3] and by anodic potentiodynamic polarisation. The measurement of the rate of accumulation of hydrogen evolved by the corroding sample was carried out for 3% NaCl solution saturated with $Mg(OH)_2$ having a pH of 10.4 at 25°C. The corroded surfaces of the samples exposed to the 3% NaCl solution for various durations were examined by SEM.

Anodic potentiodynamic polarisation was performed with an ACM potentiostat/galvanostat field machine in 0.01 M NaCl electrolyte, adjusted initially to pH 12 using 1 N NaOH. The tests were conducted at 25°C using a calomel reference electrode (SCE) with a scan rate of 1 mV s^{-1}. All potentials quoted in this paper are versus SCE. The working electrode was made by attaching Cu wires to one end of the ribbons and sealing into a glass tube with epoxy resin. The total surface area of the ribbon exposed to the solution ranged from 0.2 to 0.4 cm^2. All specimens were equilibrated for 60 min to obtain a near steady state corrosion potential. The cathodic polarisation scans were started at potentials of −1200 mV, set approximately 200mV below the E_{corr}. A fresh solution was used for each sample.

3. Results

The surface corrosion morphologies after 30 or 5 min immersion times in 3% NaCl solution saturated with $Mg(OH)_2$ of samples before and after prior heat treatment at 160°C for 4 min and 60 min are compared in Fig. 1. The corroded surfaces of the samples, as-spun (Fig. 1a) and after heat treatment for 4 min (Fig. 1b) indicate that there was only a small amount of corrosion product over the sample surface after 30 min immersion in the test solution. In contrast, the corroded surface after 5 min immersion time, of the sample heat treated for 60 min at 160°C is characterised by severe corrosive attack resulting in the formation of voluminous corrosion product as shown in Fig. 1c. The difference in the amount of corrosion products formed on the sample surfaces indicates that the samples as-spun and after heat treatment at 160°C for 4 min were

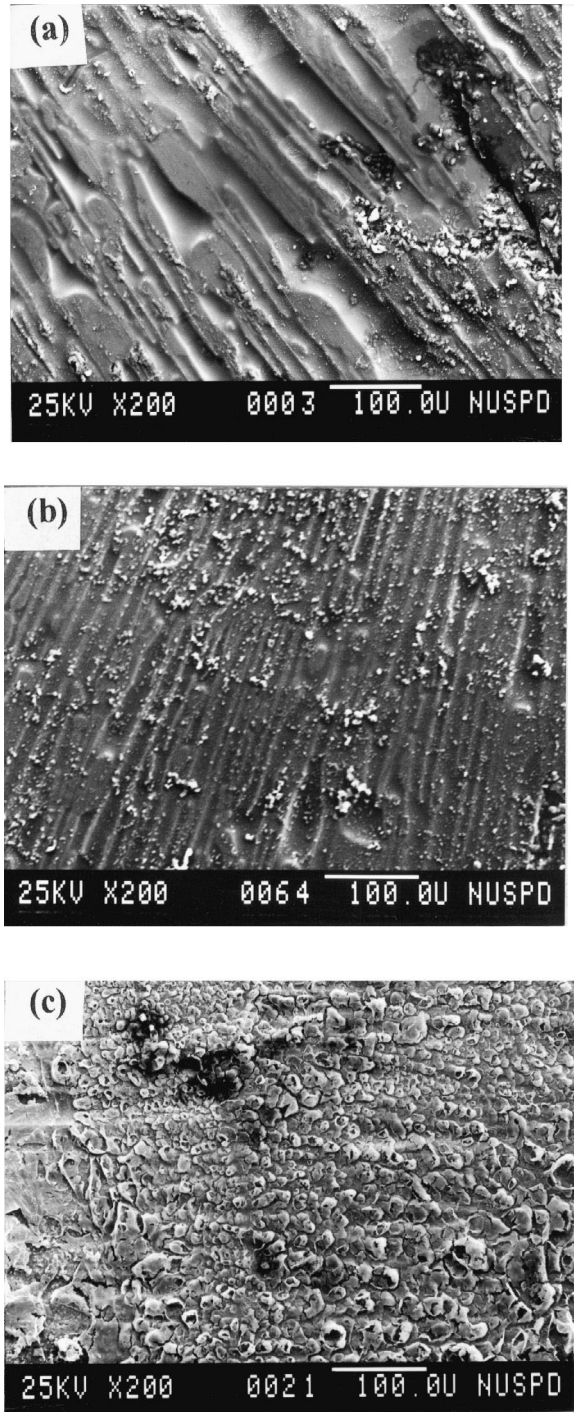

Fig. 1. SEM micrographs of chill-surfaces of $Mg_{82}Ni_{18}$ ribbon with different immersion times in 3% NaCl (a) As-spun sample, after 30 min immersion; (b) Sample, heat treated at 160°C for 4 min, after 30 min immersion; (c) Heat treated sample at 160°C for 60 min, after 5 min immersion.

more corrosion resistant in the test solution than the sample heat treated for 60 min.

The time dependence of dissolution rates as determined from hydrogen evolution of the as-spun and heat treated samples in 3% NaCl solution are shown in Fig. 2. There is a substantial difference in dissolution rates for as-spun samples and after heat treatment. For example, the dissolution rate for the as-spun sample was relatively steady at ~300 mpy. Comparison for the sample after heat treatment for 4 min, indicates that the dissolution rate was invariably lower, decreasing continuously from initial values of 110 mpy to 80 mpy in 3 h. Results for the samples heat treated beyond 10 min in contrast show that initial dissolution rates were as high as ~6000 mpy. For these samples, testing was stopped immediately after 10 min immersion as breakage of the ribbon occurred and the surface area was no longer the same as the initial surface area.

Anodic potentiodynamic scans in 0.01 M NaCl solutions for the samples as a function of heat treatment time at 160°C are shown in Fig. 3. Analysis of these scans is best performed by considering the cathodic (negative of the corrosion potential) and anodic (positive of the corrosion potential) halves separately.

For the cathodic halves of the scans, linear Tafel slopes defined as voltage change per decade change in current were detected for the as-spun (120 mV dec^{-1}) and 4 min (75 mV dec^{-1}) samples. Extrapolation of these Tafel slopes to the corrosion potentials reveals corrosion rates of 43 mpy and 31 mpy as-spun and after 4 min at 160°C respectively. The regions over which Tafel behaviour was observed were quite short (between −970 mV and −1040 mV for as-spun and −920 mV and −980 mV for the 4 min samples respectively). At more negative potentials, hydrogen gas bubbles formed as the current density approached 1 mA cm^{-2}, causing the current flowing to deviate below the expected Tafel line. Hydrogen bubbles were also the reason why no linear Tafel regions were observed from the samples heated for times longer than 4 min.

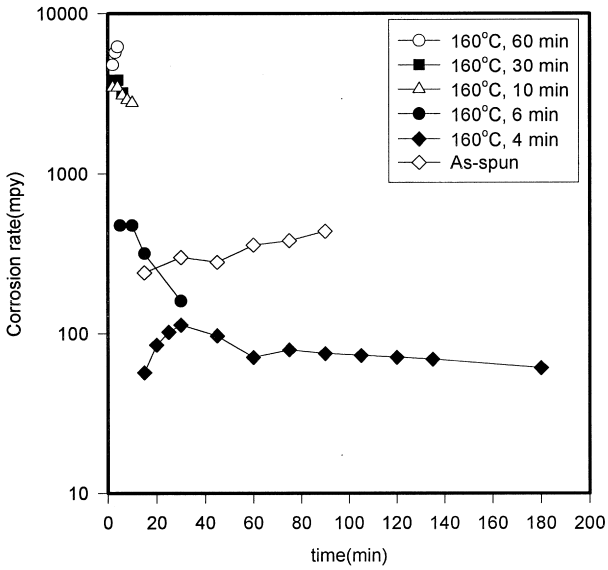

Fig. 2. Dissolution rate as a function of duration of hydrogen evolution time in 3% NaCl solution for $Mg_{82}Ni_{18}$ samples after various heat treatment times at 160°C.

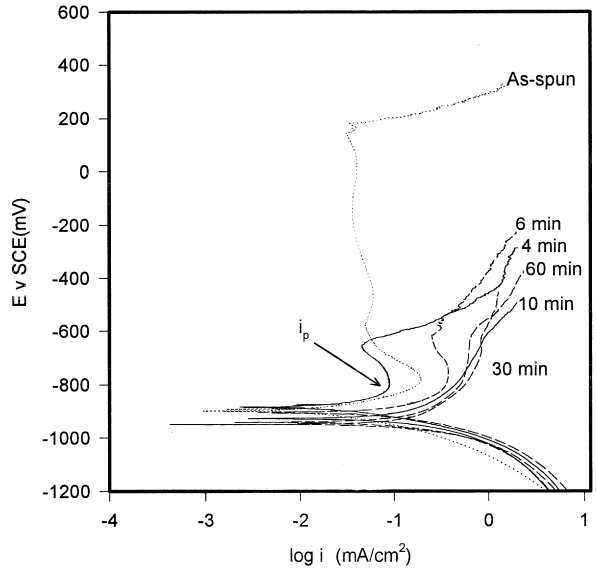

Fig. 3. Potentiodynamic polarisation scans of the $Mg_{82}Ni_{18}$ samples before and after heat treatments in 0.01 M NaCl, adjusted to pH 12 with a scan rate of 1 mV s^{-1}.

Although no Tafel regions were detected for the samples heated for times longer than 4 min, the observation from the cathodic part of the potentiodynamic scans that the hydrogen evolution rate on all the heat treated specimens does not vary greatly, means that for these samples an increase in corrosion rate should result in a negative shift in the corrosion potential. If it is assumed that the hydrogen evolution rate is the same on all the heat treated samples, estimates of their corrosion rates can be obtained from their corrosion potentials (Table 1) and the cathodic Tafel line obtained from the 4 min sample. This results in corrosion rates of 57 mpy, 106 mpy, 214 mpy, 173 mpy for the samples after heat treatments of 6, 10, 30 and 60 min respectively.

The anodic halves of the potentiodynamic scans do not show any Tafel type behaviour due to the onset passivation, which is indicative of the formation of a passive film

Table 1
Summary of corrosion data collected from the potentiodynamic scans

Sample	Corrosion potential (mV vs SCE)	Corrosion rate (mpy)	Critical passivating current density (i_p) (mA cm^{-2})
As spun	−900	43	0.20
4 min	−887	31	0.08
6 min	−907	57	0.40
10 min	−927	106	0.60
30 min	−950	214	0.80
60 min	−943	173	0.60

most likely either $Mg(OH)_2$ or MgO. The as-spun, 4 min and 6 min samples clearly showed typical active/passive transition peaks at about −800 mV.

The critical passivating current density (i_p) for the active/passive transition was invariably lower for the sample heat treated for 4 min (0.08 mA cm^{-2}) than for the as-spun sample (0.20 mA cm^{-2}). However, for longer heating times i_p was higher than for the as-spun sample, with a value at 6 min of 0.40 mA cm^{-2}.

For heat treatment times longer than 6 min it is difficult to distinguish the active/passive transition peaks as oxide breakdown appears to occur almost immediately after formation. Although some linear regions were observed after oxide breakdown, these yielded Tafel slope values greater than 400 mV dec^{-1}. Such large values are inconsistent with an electron transferred controlled reaction (theoretical maximum 120 mV dec^{-1}) and thus suggest that the corrosion in these regions is at least partially limited by the mass transport of metal ions away from the corroding surface. Corrosion rates cannot be reliably obtained by the extrapolation of Tafel lines back to the corrosion potential from potential regimes where the corrosion process is limited by mass transport.

All the heat treated samples showed oxide breakdown, followed by rapid corrosion, at potentials negative of about −650 mV, with only the as-spun sample exhibiting an extensive passive region breakdown not occurring in this case until +200 mV. The potentiodynamic scan of the as-spun sample also showed an additional small peak at about −470 mV which could possible be associated with the formation of $Ni(OH)_2$. Table 1 summarises the corrosion information derived from the potentiodynamic scans.

Fig. 4 shows a plot of the dissolution rate, as determined from both hydrogen evolution and potentiodynamic scans, and the critical passivating current density of the $Mg_{82}Ni_{18}$ samples as a function of heat treatment. Although the actual values of the electrochemical corrosion rates are less than that observed by the hydrogen gas testing method, which reflects the more benign environment used in the electrochemical tests (0.01 M NaCl, pH 12 compared to 3% NaCl, pH 10.4), the trends between the relatively corrosion rates of the different heat treatments are the same for both tests. The results indicate that for the sample heat treated at 160°C for 4 min exhibited dissolutions rates and i_p values that were invariably lower than those of the samples either untreated or provided with heat treatments beyond 6 min.

The XRD results of the samples, before and after heat treatment are shown in Fig. 5. The results indicate that the as-spun samples were fully amorphous. Heat treatment of the samples at 160°C for the various durations resulted in the transition from the fully amorphous, through partially crystallised and finally to fully crystallised states. It can be seen that heat treatment at 160°C for 4 min (curve b in Fig. 5) resulted in a partially crystallised alloy, with prominent reflections corresponding to Mg_2Ni phase and an unknown

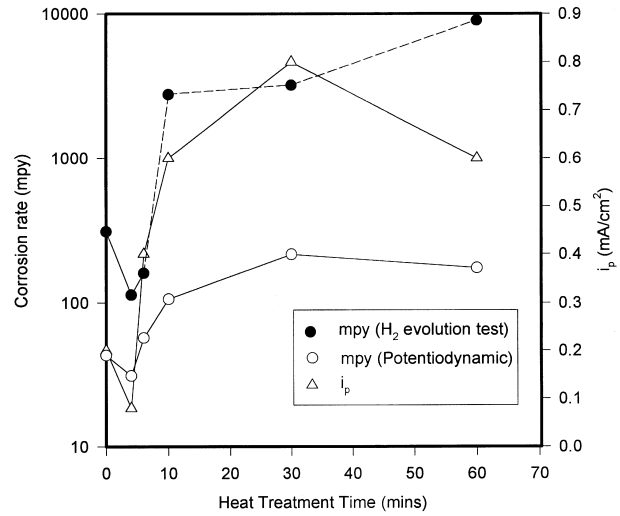

Fig. 4. Dissolution rate (mpy), as determined from both hydrogen evolution and potentiodynamic scans, and the critical current density (i_p) at the onset of passivation for $Mg_{82}Ni_{18}$ ribbon as a function of heat treatment time. Except for samples treated at durations above 10 min, dissolution rates measured from hydrogen evolution were taken after 30 min immersion. Average dissolution rates were used for samples heat treated at 160°C above 10 min.

phase superimposed onto the amorphous pattern. With the extension of heat treatment to 10 and 60 min as shown in curves c and d, the fully crystallised sample consisted of the phases of Mg, Mg_2Ni and the unknown phase.

Fig. 6 shows the DSC crystallisation curves of the fully amorphous and residual amorphous phase of the as-spun and heat-treated samples respectively. For the fully amorphous sample, the crystallisation takes place with a large exothermic peak followed by a relatively shallow and overlapping exothermic peak (curve a). With heat treatment at 160°C for 4 min, the crystallisation of the residual

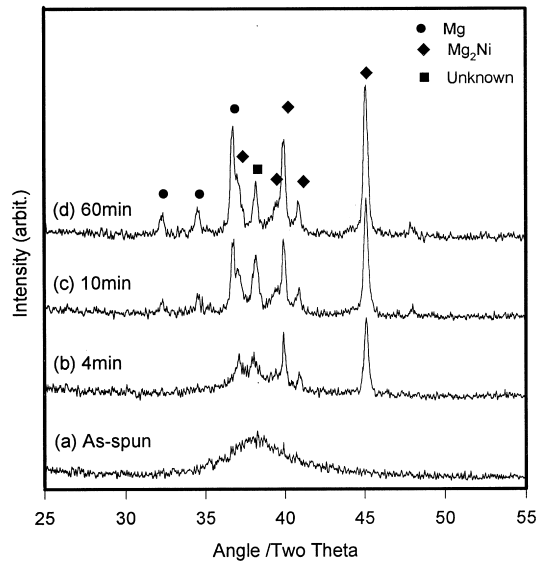

Fig. 5. XRD results for the $Mg_{82}Ni_{18}$ ribbons after different heat treatments at 160°C. (a) as-spun (b) 4 min (c) 10 min (d) 60 min.

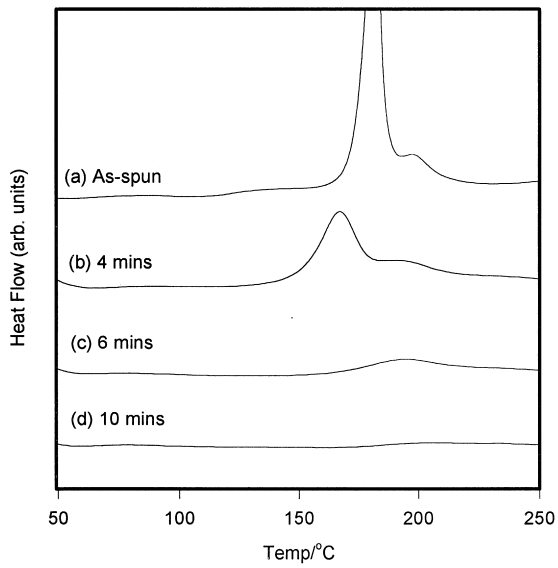

Fig. 6. DSC results for the $Mg_{82}Ni_{18}$ ribbons after different heat treatments at 160°C. (a) as-spun (b) 4 min (c) 6 min (d) 10 min.

amorphous phase occurred with a decreased exothermic peak as shown in curve b. With the heat treatment time extended to 6 min (curve c), the crystallisation occurred with the absence of the main exothermic peak. Curve d shows that for the sample heat treated at 160°C for 10 min, no obvious crystallisation behaviour was observed. The decreasing magnitude of the exothermic peaks with the duration of heat treatment indicates a decreasing amount of the amorphous phase, which is consistent with the XRD results (Fig. 5).

Fig. 7a shows a TEM micrograph of the as-spun $Mg_{82}Ni_{18}$ ribbon displaying a featureless matrix. The typical intense amorphous ring in the corresponding diffraction pattern in Fig. 7b confirm that the as-spun sample was fully amorphous. For the partially crystallised structure obtained after heat treatment at 160°C for 4 min as shown in Fig. 7c, revealed that there were rod-like precipitates present in the featureless matrix. Fig. 7d shows the diffraction pattern taken from the area in Fig. 7c. According to the indexing shown in Fig. 7e, the precipitates were identified as the Mg_2Ni phase. Treatment of the sample at 160°C for 60 min results in the formation of the precipitates in a lamellar two-phase matrix (Fig. 7f). The corresponding diffraction pattern (Fig. 7g) with indexing (Fig. 7h) indicates that Mg_2Ni and Mg were present. It is noted that the measured unknown d-spacing of 2.37 from both the diffraction rings of the partially crystallised (Fig. 7d) and fully crystallised (Fig. 7g) samples were consistent to the XRD results (Fig. 5).

4. Discussion

The Mg-rich side equilibrium binary Mg–Ni phase diagram shows a eutectic reaction of αMg and Mg_2Ni at 11.3 at% Ni at temperature of 506°C [15]. Thus it is expected that αMg and Mg_2Ni phase will be present in our sample with 18at% Ni after sufficient heat treatment (Figs. 5 and 7) However, the reflection at $d=2.37$ Å in Figs. 5 and 7 belongs to neither αMg nor Mg_2Ni, indicating presence of an unknown phase in our sample. It is noted that an unknown phase, consisting of mainly Mg and Ni with similar d-spacing was also reported in binary Mg–Ni

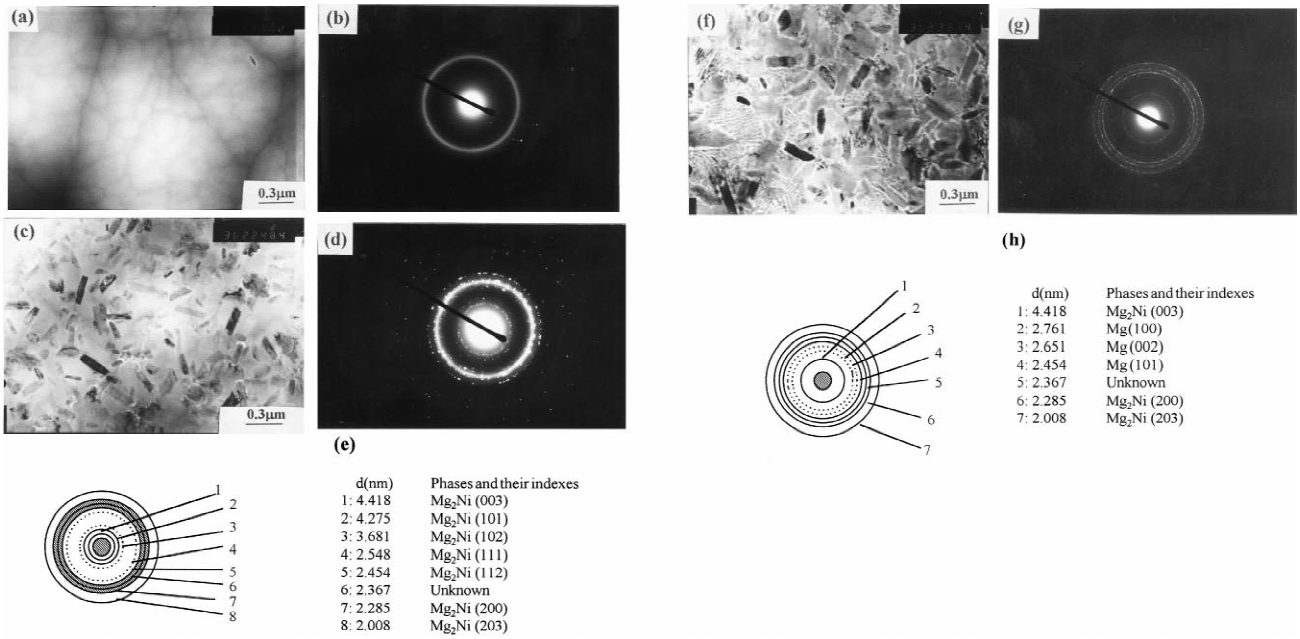

Fig. 7. Bright field TEM micrographs and corresponding diffraction patterns of $Mg_{82}Ni_{18}$ ribbons heat treated under the following conditions: (a, b) as-spun; (c, d) 160°C for 4 min, (e) corresponding indexing of (d); (f, g) 160°C for 60 min, (h) corresponding indexing of (g).

melt-spun ribbons and exists up to the melting temperature [16]. In the same report this unknown phase was also present together with αMg, Mg_2Ni and $CaMg_2$ in a ternary amorphous $Mg_{85}Ni_{10}Ca_5$ melt-spun ribbon after annealing at 205, 250 and 463°C. However, identifying this phase would have required the use of detailed XRD, TEM and compositional analysis.

The detrimental effects of metallic impurities on the salt water corrosion resistance of crystalline Mg and its alloys have been extensively studied by Hanawalt et al. [1]. In their study, they have reported a tolerance limit for Ni, Fe or Cu in the Mg based crystalline alloy, above which the corrosion rate increases dramatically. The study showed that when the amount of these elements exceeds a tolerance value, typically 100 ppm, the corrosion rate in 3% NaCl increased sharply to over 2000 mpy. Although the current sample has a much higher Ni content than 100 ppm, the hydrogen evolution results show that the dissolution corrosion rate for the fully amorphous as-spun alloy is well below 2000 mpy (Fig. 2). Moreover, the present results for the Mg–Ni binary fully amorphous ribbon is consistent with the previous reports for ternary Ni containing Mg–Ni–Nd fully amorphous alloys [13]. The low dissolution rate of these high Ni containing alloys can be attributed to the fact that they are fully amorphous so that no Ni containing particles were present and all Ni atoms are embedded in the Mg matrix. The results do suggest that the detrimental effects of Ni can be significantly reduced if the microgalvanic effect is eliminated even when the Ni content in the Mg alloy is high.

The major observation reported in this work is the enhanced corrosion resistance for the partially crystallised samples. For example, after heat treatment at 160°C for 4 min, the XRD (Fig. 5) and the TEM results (Fig. 7c and Fig. 7d) showed that large amounts of rod-like Mg_2Ni were present in the amorphous matrix. However, the corrosion rate was one-third that of the fully amorphous as-spun sample (Fig. 2). This result is consistent with our previous result [14] that the microgalvanic coupling between the Mg_2Ni phase and the residual amorphous matrix was not as active compared to that of the coupling between the Mg matrix and the Mg_2Ni phases in the fully crystallised alloy. Alternatively, it could be that for the partially crystallised samples the increased thermodynamic stability offered by crystallisation initially outweighs the disadvantages of microgalvanic coupling. However, as crystallisation proceeds the microgalvanic effect starts to dominate.

The electrochemical polarisation results (Fig. 3) indicate that the kinetics of the hydrogen evolution reaction are slower on the amorphous surface than on the partially crystalline surfaces. The Tafel slope of 120 mV dec^{-1} observed for the hydrogen evolution reaction on the as-spun sample is consistent with the rate limiting step being the initial adsorption of a hydrogen atom on to the metal surface;

$$M + H_2O + e^- \rightarrow M - H_{ads} + OH^- \text{ (aq)} \quad (1)$$

rather than either of the two possible desorption steps [17]

$$2M - H_{ads} \rightarrow 2M + H_2 \quad (2)$$

$$M - H_{ads} + H_2O + e^- \rightarrow M + H_2 + OH^- \text{ (aq)} \quad (3)$$

both of which result in lower Tafel constants being observed, ideal values at low overpotentials being 30 mV dec^{-1} and 40 mV dec^{-1} when reactions Eq. (2) or Eq. (3) respectively are rate determining. The intermediate value of the Tafel slope of 75 mV dec^{-1} observed on the sample heat treated for 4 min suggests that hydrogen evolution reaction is under mixed control, with neither the adsorption or desorption steps individually determining the overall rate of reaction. This suggests that the adsorption reaction Eq. (1) occurs at a faster rate on the heat treated surfaces, and this is consistent with the cathodic part of the potentiodynamic scans, which indicate that the kinetics of the hydrogen evolution reaction are between 2 and 3 times faster on the heat treated samples than on the as-spun sample. The lower corrosion rate observed with the as-spun sample than the heat treated samples (with the exception of short <6 min heating times), may be due in part to decrease in kinetics of the hydrogen adsorption onto the former amorphous surface.

The electrochemical results also showed that for the partially crystallised sample obtained after 4 min heat treatment the critical passivating current density was lower than for the fully amorphous sample. This suggests that the presence of Mg_2Ni phases in the 4 min sample, as shown by XRD (Fig. 5) and TEM (Fig. 7c and Fig. 7d), aids the formation of the passive film. However, longer heat treatment times resulted in critical passivating current densities higher than that of the fully amorphous sample. XRD (Fig. 5) and TEM (Fig. 7f and Fig. 7h) showed that at times longer than 4 min Mg phases begin to form. The electrochemical results thus suggest that these phases are detrimental to the formation of a passive film.

Furthermore, the potentiodynamic scans showed that only the fully amorphous sample had an extended passive regime, with all the heat treated samples showing a return to active corrosion at potentials positive of -650 mV. It is suggested that formation of crystals of the Mg_2Ni phases in the amorphous matrix, as seen in the XRD (Fig. 5) and TEM (Fig. 7c and Fig. 7d) results, introduces surface segregation and renders the samples more susceptible to localised corrosion at the boundaries of these phases. Further growth of Mg_2Ni phases and the precipitation of Mg phases with increasing heat treatment times results in the formation of more boundary regions and thus increases the susceptibility to localised corrosion.

From the above results, it is observed that crystalline Mg_2Ni present on a sufficiently fine scale in an amorphous matrix is protective in that it both reduces the open-circuit corrosion rate and helps the formation of a protective

passive film under mildly oxidising conditions. However, the presence of such crystalline phases drastically reduces the ability of the alloy to maintain passivity under strongly oxidising conditions.

5. Conclusion

Amorphous $Mg_{82}Ni_{18}$ alloys, partially crystallised by heat treatment give enhanced corrosion resistance compared to the untreated sample, whereas fully crystallised specimens exhibited poor corrosion resistance. The former result is associated to the low corrosion current between the finely distributed Mg_2Ni phase and the amorphous matrix. The latter result, on the other hand, is attributed to microgalvanic action between the crystallised Mg and Mg_2Ni phases then present.

Acknowledgements

The authors would like to extent their appreciation to Prof. H. Jones for the Mg–Ni ingots that were used as starting materials for the melt spinning. Thanks are due also to Madam G.L. Loy for her technical help in the area of Transmission Electron Microscopy.

References

[1] J.D. Hanawalt, C.E. Nelson, J.A. Peloubet, Trans. AIME. 147 (1942) 273.
[2] D. Rugg, R.G.J. Edyvean, H. Jones, Mater. Sci. Tech. 9 (1993) 994.
[3] J.D. Cotton, J. Electrochem. Soc. 136 (1989) 523C.
[4] G.L. Maker, J. Kruger, J. Electrochem. Soc. 137 (1990) 414.
[5] G.L. Maker, J. Kruger, K. Sieradzki, J. Electrochem. Soc. 139 (1992) 47.
[6] S. Krishnamurty, M. Khobaib, E. Robertson, F.H. Froes, Mat. Sci. Eng. 99 (1988) 507.
[7] F. Hehmann, F. Sommer, H. Jones, R.G.J. Edyvean, J. Mat. Sci 24 (1989) 2369.
[8] D.S. Ahmed, R.G.J. Edyvean, C.M. Sellars, H. Jones, Mat. Sci. Tech. 6 (1990) 469.
[9] Y. Li, J. Lin, F.C. Loh, K.L. Tan, H. Jones, J. Mat. Sci. 31 (1996) 4017.
[10] Y. Li, J. Lin, F.C. Loh, K.L. Tan, G.L. Chen, C.H. Kam, J. Mat. Sci. 33 (1998) 1075.
[11] P.L. Miller, B.A. Shaw, R.G. Wendt, W.C. Moshier, Corrosion 51 (1995) 922.
[12] S.J. Dobson, I. Whitaker, H. Jones, H.A. Davies, in: G.W. Lorimer (Ed.), Proceedings of the Third International Magnesium Conference, The Institute of Materials, Manchester, UK, 1996, p. 507.
[13] Y. Li, S.C. Ng, C.H. Kam, Mater. Lett., in press.
[14] C.H. Kam, Y. Li, S.C. Ng, A. Wee, J.S. Pan, H. Jones, J. Mat. Res., submitted.
[15] A.A. Nayeb-Hashemi, J.B. Clark, Phase Diagrams of Binary Magnesium Alloys, Metals Park, Ohio, ASM Int., 1988, pp. 219–225.
[16] T. Shibata, A. Inoue, T. Masumoto, J. Mater. Sci. 28 (1993) 379.
[17] Southampton Electrochemistry Group: R. Greef, R. Peat, L.M. Peter, D. Pletcher, J. Robinson, in: Instrumental Methods in Electrochemistry, Ellis Horword, Chichester, UK, 1985, pp. 233–241.